ingegneria sismica
International Journal of Earthquake Engineering
Anno XLIII - Num. 1 - 2026

Study on the impact of electric vehicle charging and switching modes on the temporal and spatial distribution of grid loads based on big data analysis

Tao Luo[1,*], *Bo Li*[1], *Ruiguang Ma*[2], *Tiannan Ma*[2], *Qiang Ye*[2] *and Hao Luo*[2]

[1] State Grid Sichuan Electric Power Co., Ltd., Chengdu, Sichuan, 610041, China
[2] State Grid Sichuan Electric Power Company Economic and Technological Research Institute, Chengdu Sichuan, 610041, China

SUMMARY: *With the widespread adoption of electric vehicles, the distinct features of their charging and switching technologies have a significant impact on the grid load. This paper focuses on the operation mechanism of charging and switching technologies, and after analyzing the temporal and spatial patterns of load variation in EV charging and switching modes, a Monte Carlo simulation method based on the momentary charging likelihood is adopted to establish a charging load prediction model to investigate the temporal–spatial distribution patterns of charging demand under different day categories, vehicle types, charging and switching modes, and charging areas. Example analysis shows that the model can accurately simulate the user's travel pattern, capturing the temporal and spatial variation in charging and battery-swapping demand for electric vehicles across different driving and parking states. The charging load distribution of various vehicle categories varies greatly, while the charging loads of private cars and cabs account for a higher proportion, with higher regulation potential; compared with double holidays, the charging demand fluctuates more on weekdays, with a higher total demand; the charging demand also has obvious seasonal characteristics, with a greater demand in winter and summer, and the peak appears in an earlier time. The study offers a reference for the planning and development of electric vehicle charging facilities as well as for assessing their impact on the power grid.*

KEYWORDS: *electric vehicle; grid load spatial and temporal distribution; Monte Carlo simulation; charging and switching mode; charging load forecasting model*

1 Introduction

As global energy-related challenges become increasingly prominent, the ecological environment deteriorating, and people becoming more and more aware of energy saving and ecological conservation, the electric vehicle industry has ushered in fresh growth opportunities [1, 2]. As a kind of green transportation, electric vehicles have important strategic significance in ensuring national energy security, alleviating pollution in urban areas and promoting economic development and industrial structure adjustment [3-5].

The application and deployment of large-scale electric vehicles is expected to exert a certain impact upon the traditional power grid, and existing relevant research generally focuses on the three aspects covering electric vehicle charging and discharging load prediction, the related impact of electric vehicle grid integration on the power grid load, and the optimal scheduling

*becautious22@163.com
https://doi.org/10.65102/is2026135
Published: 30 April, 2026

of electric vehicle charging and discharging [6-8]. Among them, for the research on the previous two aspects, experts and scholars have made a large number of research results, analyzing historical charging load profiles of electric vehicles through simulation modeling, and estimating the load amount associated with electric vehicles and analyzing its impact through neural network simulation, grey simulation simulation, and support vector machine prediction [9-12]. The entry of electric vehicles into the power grid is expected to exert a serious influence on the grid load, and it is important that analysts examine the load of electric vehicle charging and switching modes from both time and space levels for the planning of future spatial and temporal layouts of electric vehicle charging stations in the future [13, 14].

The deepening of smart grid research and the quantitative popularization of EVs have accumulated a substantial volume of electricity consumption data in the process, and the continuous updating of a variety of advanced ideas and smart technologies have resulted in an increasing and complex study regarding the influence of electric vehicles upon the grid load [15, 16]. Meanwhile, at this stage, the level of grid intelligence continues to improve, the complexity of the basic data applied to the analysis of the spatial and temporal distribution characteristics of load patterns continues to increase, a richer range of influencing factors are taken into account and involved in the calculation, and the data storage and computing scale grows rapidly, gradually constituting the grid load analysis with big data [17-19]. Concurrently, advances in big data analytics improve the real-time reliability of grid load data collection, opening up new possibilities for investigating the effects of load spatiotemporal variation [20].

In this paper, through a large number of research on the charging demand of existing pure electric vehicle charging/exchange stations, the data characteristics of the charging load of pure electric vehicle charging stations are analyzed, and the primary determinants affecting pure electric vehicle exchange stations are determined. On this basis, the geospatial constraints on charging infrastructure deployment and the situation of EV users' mileage anxiety are fully considered, the charging and switching decision-making mechanism is formulated, and a probability distribution fitting model of charging behavior is established based on the travel chain and travel probability matrix method using multiple probability distribution forms, and a charging demand forecasting framework is established based on the Monte Carlo simulation method of moment-to-moment charging probability. Finally, the spatial and temporal distribution of grid load under EV charging and switching mode is simulated, and a region-specific charging load forecast is obtained, which provide a reference basis for related scholars to study in depth the role played by EVs in grid interaction.

2 Characterization of temporal and spatial loads in electric vehicle charging and switching modes

2.1 Cyclical and volatility analysis

The operation of EV vehicle charging/exchange stations is fixed within a specific time span, making variations in charging loads at charging stations inherently regular, mainly in terms of daily periodicity.

2.1.1 Daily periodicity

Daily periodicity in charging load refers to the regular pattern manifested by load fluctuations within a 24-hour cycle. Figure 1 shows the charging load data for three months from July to September 2022 for an electric vehicle. From the diurnal load profile, it is evident that the electric vehicle charging/exchanging station starts to have charging load at about 8:00 every

day, and the peak load appears between 12:00 and 14:00 and between 18:00 and 19:00, and all charging is basically completed after 23:00, when it starts to have no load, and it lasts until about 8:00 the next day.

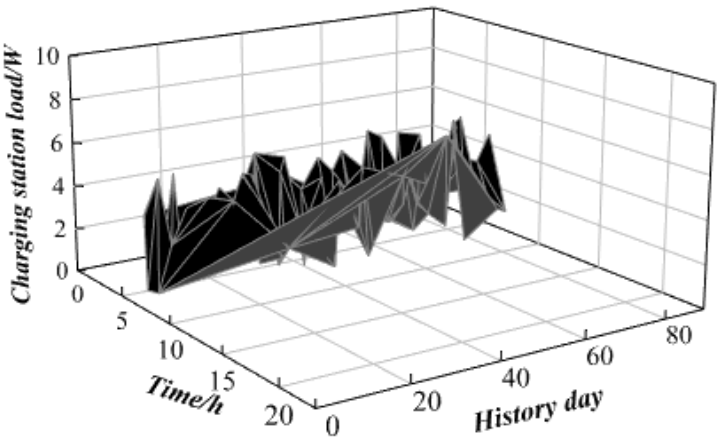

Figure 1: Three months of electric car charging station day load curve

2.1.2 Volatility analysis

In this paper, the stochasticity and volatility of charging loads in electric vehicle exchange stations are characterized by daily average load (L_{mean}), daily maximum load (L_{max}), short-time average rate of change of daily load (CR_{mean}), short-time maximum rate of change of daily load (CR_{max}), average rate of change of loads between adjacent days (CA_{mean}) and maximum rate of load variation between adjacent days (CA_{max}). The load characterization indexes of EVSE for the whole month of November are shown in Table 1.CR reflects the rate of change of load every 15 minutes. As indicated in the table, the daily average load at the electric vehicle exchange station shows an upward and downward fluctuation in 190kW, the daily maximum load changes in the range of 600kW~850kW, the daily maximum short-time change rate of the load fluctuates up and down in 55%, and the short-time maximum change rate of the daily load reaches more than 100% on some days, and the maximum change rate of the load on the two neighboring days is as small as 66.72%, and the largest reaches nearly 199.21%, which is a large change rate. 199.21%, a large variation. This shows that the EV charging and battery-swapping load is highly random and exhibits strong volatility, which increases the difficulty of prediction

Table 1: The performance of the power station for the whole of November

Date	L_{mean} 10^5W	L_{max} 10^5W	CR_{mean} %	CR_{max} %	CA_{mean} %	CA_{max} %
November 1st	2.44	8.28	7.17	118.88	18.52	101.38
November 2nd	1.71	7.35	7.89	32.9	14.24	71.33
November 3rd	1.88	8.02	7.67	47	29.67	145.61
November 4th	2.14	7.59	7.53	42.3	14.52	198.91
November 5th	2.24	6.52	7.38	31.16	29.55	121.47
November 6th	2.48	7.18	6.2	38.03	15.77	127.24
November 7th	2.35	6.91	7.69	76.85	11.25	151.63
November 8th	2.04	7.9	6.33	50.14	11.45	70.56
November 9th	2.03	7.62	7.76	59.39	13.72	157.63
November 10th	2.2	7.47	7.22	45.63	21.47	130.7
November 11th	2.49	8.32	7.53	47.59	13.3	146.11
November 12th	2.37	7.81	6.09	73.94	14.55	182.28
November 13th	2.43	8.14	6.99	36.15	24.23	84.21
November 14th	2.19	7.25	5.76	39.59	22.41	148.68
November 15th	1.74	7.72	6.66	58.74	23.4	169.47
November 16th	2.38	7.59	6.98	76.77	26.66	106.12
November 17th	2.29	8.4	7.96	45.36	15.84	149.78
November 18th	2.14	6.64	5.52	64.46	19.57	96.02
November 19th	2.37	7.02	5.7	53.65	27.63	144.61
November 20th	2.03	7.1	7	65.55	18.4	114.4
November 21st	2.31	6.9	7.15	49.69	11.13	66.72
November 22nd	1.93	8.08	5.68	71.77	11.9	76.2
November 23rd	1.78	6.66	6.29	48.82	16.84	95.71
November 24th	1.71	6.89	5.87	43.85	17.28	91.51
November 25th	1.92	7.92	7.38	71.04	14.66	199.21
November 26th	1.84	7.16	5.92	65.79	27.94	192.03
November 27th	2.11	8.23	6.01	30.92	13.18	84.55
November 28th	2.39	8.44	7.88	37.24	19.14	75.36
November 29th	1.88	7.44	6.53	48.41	18.78	186.32
November 30th	2.21	8.33	10.08	220.52	30.78	85.17

2.2 Analysis of relevant factors

The Pearson correlation coefficient, also referred to as the Pearson product-moment correlation ratio, serves as a tool for measuring the relationship between different variables X and Y during the period of time, and its value usually lies in the -1 and 1 interval.

The Pearson correlation coefficient between two variables is computed as the ratio of the covariance to the standard deviation between the two variables:

$$\rho X,Y = \frac{cov(X,Y)}{\sigma X \sigma Y} = \frac{E\left[(X-\mu X)(Y-\mu Y)\right]}{\sigma X \sigma Y} \tag{1}$$

where X and Y represent two variables respectively, $cov(X,Y)$ denotes the covariance between the two variables. The above equation defines the overall coefficient of interest and uses the Greek lower case letter ρ as a representative symbol. Computing the covariance

coefficients and standard deviations of the samples yields the Pearson's correlation coefficient and can be denoted by the English lower case letter r :

$$r = \frac{1}{n-1}\sum_{i=1}^{n}\left(\frac{\bar{X} - X_i}{\sigma X}\right)\left(\frac{\bar{Y} - Y_i}{\sigma Y}\right) \tag{2}$$

The Pearson correlation coefficient falls within the range of -1 to 1. A maximum value of 1 for the coefficient indicates that both X and Y can be well described through a linear equation, that any of the data points fall exactly on the same straight line, and that Y rises as X increases. A coefficient with a value in the range -1 means that all data points fall on the straight line and Y decreases as the distance X increases. A constant value of 0 for the coefficient implies that there is no linear relationship between the different variables.

The validation of Pearson's correlation coefficient is generally divided into 3 steps:

1. Confirm the existence of association between two datasets

Pearson's correlation coefficient also applies to linear relationships between different variables that are both continuous data. Or the overall of different variables are normally distributed, or approximately normal with a single peaked distribution. Or the observations of the different variables are in pairs and the pairs of observations are independent of each other.

2. Identify the overall mean and variance of two sets of data

Complete the statistics and utilize the mathematical formulas to calculate the overall mean and variance of two sets of data.

3. verify Pearson's correlation coefficient

The mean and variance of both datasets are substituted into the above formula to obtain the value of Pearson's correlation coefficient between the two sets of data. When the value of r is greater than 0, it implies that the different variables are positively associated, i.e. the greater the change in one will be the greater the change in the other. When the value of r is less than 0, it implies that the different variables are negatively associated, i.e., the greater the change in one variable, the smaller the change in the other variable will be. When r is zero, it implies that the variables share no linear relationship, but can be correlated in other ways.

2.2.1 Correlation analysis between load and temperature

The value of the correlation coefficient r has a certain range, i.e., when $|\boldsymbol{r}|\leq 1$. When $|\boldsymbol{r}|=1$, it means that the maximum temperature and the daily average load are perfectly linear, i.e., it is a definite functional relationship. When $|\boldsymbol{r}|=0$, it implies that no linear relationship exists between the maximum temperature and the daily average load, but this does not mean that there is no other form of relationship between the maximum temperature and the average daily load. When $0<|\boldsymbol{r}|<1$, it indicates that there are varying degrees of linearity between the maximum temperature and daily average load. It is usually considered that $0<|\boldsymbol{r}|<0.3$ is a weak correlation, $0.3\leq|\boldsymbol{r}|<0.5$ is a low correlation, $0.5\leq|\boldsymbol{r}|<0.8$ is a significant correlation, and $0.8\leq|\boldsymbol{r}|<l$ is a high correlation. Figure 2 shows the scatter distribution of daily average load and maximum temperature. By calculation, a correlation coefficient of 0.8012 is obtained between the daily maximum temperature and the daily average load, indicating a strong association between the maximum temperature and the daily average load. In summer when the temperature increases, the charging load also increases. This can be explained by the fact that the hot weather and the air conditioning of electric vehicles speed up the consumption of electric energy, which ultimately leads to an increase in the charging load.

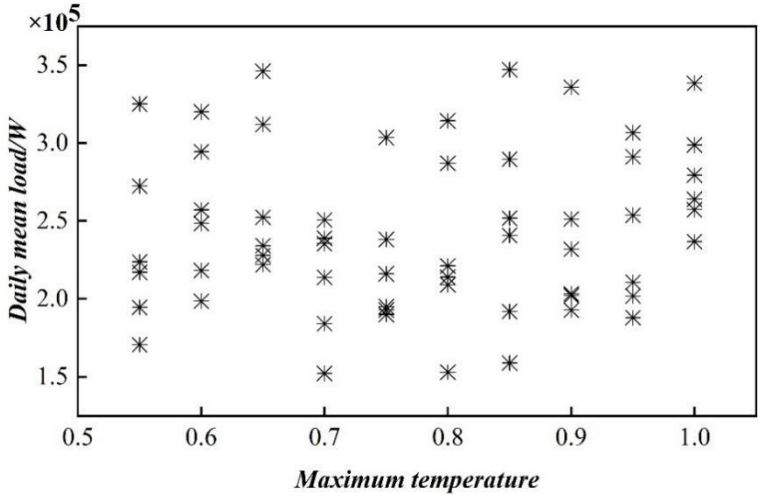

Figure 2: Average load and maximum temperature scatter distribution

2.2.2 Load and day types and weather conditions

Day type and weather conditions influence the behavioral patterns of the users, which consequently affects the charging load at the charging station. Tables 2 and 3 show the load analysis for different day types and weather conditions, respectively. From Table 2, it is evident that the effect of day type on the charging station load is not significant, which is due to the fact that there is not much difference in the scheduling arrangement of EVs between weekdays and non-workdays. However, in the future, if the scheduling arrangement is changed, the travel pattern of EVs is different for different day types, which in turn affects the charging load profile of the charging station. In order to enhance the generalizability of the model presented in this paper, the effect of day type is taken into account. From Table 3, it can be seen that rain and no rain have a certain effect on the charging load of charging stations, and the charging load of charging stations on rainy days is smaller than that on no rain days. So the variables considered in this study are maximum temperature, day type and weather conditions.

Table 2: Different day type load analysis

Day type	L_{mean} 10^5W	L_{max} 10^5W
Monday	7.8859	2.5152
Tuesday	8.1212	2.3381
Wednesday	8.3354	2.4456
Thursday	7.6818	2.3235
Friday	8.0125	2.3819
Saturday	8.1164	2.3657
Sunday	7.7623	2.3668

Table 3: Analysis of different weather conditions

Weather condition	L_{mean} 10^5W	L_{max} 10^5W
Rain	7.6682	2.2879
No rain	8.0155	2.4543

Since the measures of each characteristic quantity differ from one another, it is necessary to perform corresponding mappings of each physical quantity to map the values of varying measures to a specific interval, so that there can be numerical comparability between the

quantities, thus facilitating the quantitative calculation of similarity and difference. Therefore, it is necessary to establish a mapping function and a mapping database. In this paper, the normalized value of maximum temperature and the mapped values of day type and weather conditions are used as feature quantities to select similar days.

3 Impact of electric vehicle charging and switching modes on the spatial and temporal distribution of grid loads

3.1 Spatial and Temporal Characteristics of Electric Vehicle Travel

3.1.1 Probability distribution of travel time

When an EV starts a day's activity according to the rules of the travel chain, if it arrives at one of the activity phases, its arrival time as well as the next phase travel time can be obtained from the statistics.The Weibull function has a great flexibility and adaptability in fitting stochastic data, so in this section, we use the three-parameter Weibull distribution model to calibrate the time of the first trip of the EVs:

$$\begin{cases} f(t_{lea}^0;k,c,\gamma)=\left(\dfrac{k}{c}\right)\left(\dfrac{t_{lea}^0-\gamma}{c}\right)^{k-1} e^{-\left(\frac{t_{lea}^0-\gamma}{c}\right)^k}, t_{lea}^0-\gamma>0 \\ F(t_{lea}^0;k,c,\gamma)=1-e^{-\left(\frac{t_{lea}^0-\gamma}{c}\right)^k}, t_{lea}^0-\gamma>0 \end{cases} \tag{3}$$

where t_{lea}^0 denotes the moment when the EV leaves the residential area for the first time, and k,c,γ denotes the weibull shape, scale, and location parameters, where c unit is min.

When the EV travels according to the travel chain, it travels in the urban road network at a certain speed, and its average elapsed time through each road section is:

$$\overline{T}_r=\frac{L_r}{\overline{v}_r} \tag{4}$$

where $\overline{T}_r$ denotes the time taken by the EV to pass through a road of length L_r. $\overline{v}_r$ denotes the average speed in km/h, which is affected by road attributes, traffic conditions, etc., and is taken as a segmented function following (5), in km/h. i.e:

$$F(\overline{v}_{road})=\begin{cases} \dfrac{\overline{v}_r-v_{\min}}{v_a-v_{\min}}, & v_0\le\overline{v}_r<v_a \quad \text{Crowded} \\ \dfrac{\overline{v}_r-v_a}{v_b-v_a}, & v_a\le\overline{v}_r<v_b \quad \text{Moderately crowded} \\ \dfrac{\overline{v}_r-v_b}{v_c-v_b}, & v_b\le\overline{v}_r<v_c \quad \text{Normal} \\ \dfrac{\overline{v}_r-v_c}{v_d-v_c}, & v_c\le\overline{v}_r<v_d \quad \text{Moderately smooth} \\ \dfrac{\overline{v}_r-v_d}{v_{\max}-v_d}, & v_d\le\overline{v}_r<v_{\lim} \quad \text{Smooth} \end{cases} \tag{5}$$

where $v_{\min}, v_{\max}$ denotes the minimum and maximum speed of EV on the road. v_a, v_b, v_c, v_d denote the average speed of EV under different traffic congestion factors.

Generally speaking, when EV starts from the initial location and arrives at the end point that the vehicle needs to reach, the EV owner often chooses different path planning according to his needs in the current situation, such as the shortest time, the shortest distance, etc. At this time, it is necessary to use the path planning algorithm to analyze the established road network model to find the most suitable path.

3.1.2 Parking time

When an EV reaches any place in the travel chain, it is bound to stay for a period of time, which is defined in this section as the stopping time. When the EV stops in residential areas, the stopping time obeys the weibull distribution. When stopping in work and commercial areas, the stopping time t_p^d obeys a generalized extreme value distribution as in equation (6):

$$\begin{cases} f(t_p^d) = \left(\dfrac{k}{c}\right)\left(\dfrac{t_p^d}{c}\right)^{k-1} e^{-\left(\frac{t_p^d}{c}\right)^k} \\ f(t_p^d) = \dfrac{1}{\sigma}\left[1+\xi\left(\dfrac{t_p^d-\mu}{\sigma}\right)\right]^{-\frac{1}{\xi}-1} e^{-\left\{\left[1+\xi\left(\frac{t_p^d-\mu}{\sigma}\right)\right]^{-\frac{1}{\xi}}\right\}} \end{cases} \tag{6}$$

The first trip time t_{lea}^0 is determined by Eq. (3) when the EV reaches the destination d at a certain stage in the travel chain:

$$t_{arr}^d = t_{lea}^0 + \sum_{i=0}^{d-1} \Delta T_{i,i+1} + \sum_{i=1}^{d-1} t_p^i \tag{7}$$

The departure time from that point to the destination $d+1$ is:

$$t_{lea}^d = t_{lea}^0 + \sum_{i=0}^{d-1} \Delta T_{i,i+1} + \sum_{i=1}^{d} t_p^i \tag{8}$$

3.1.3 Volume of private car and cab trip characteristics

(1) Characteristic volume of private car travel

Users depart from the residential area H (Home area), and the destination is dominated by the work area W (Work area), commercial area and recreation area. The commercial area and leisure area are collectively categorized as the recreation area R (Recreation area), and it is considered that EVs travel between the 3 types of functional areas. In this paper, 3 typical travel chains are employed to describe the travel characteristics of private cars as shown in Fig. 3.

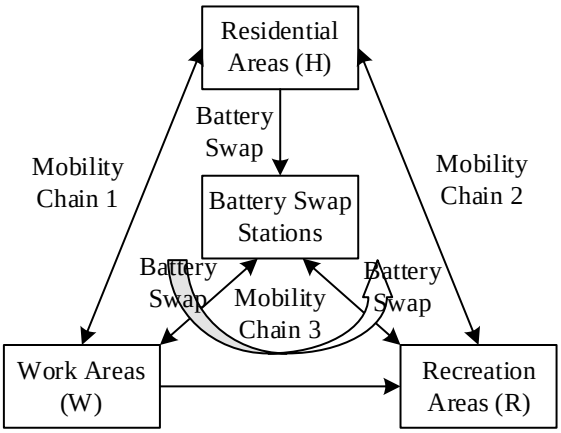

Figure 3: Typical travel pattern diagram

Trip chain 1 indicates that the user travels from the residential area toward the work area and returns to the residence when the work is finished. Trip chain 2 indicates that the traveler goes to other areas and returns to the residential area after shopping and entertainment. Trip chain 3 indicates that the traveler arrives at the work area from the residential area, and then travels to other areas for shopping and entertainment when the work is finished, and finally returns to the residential area.

The private vehicle trip characteristic quantities include the starting travel moment, stopping time, travel distance and initial charge state. Grasping the laws of these four characteristic quantities can accurately describe the daily travel process of electric vehicles. The Gaussian probability density function takes the form of equation (9):

$$y = \sum_{k=1}^{M} a_k \exp\left[-\left(\frac{x - b_k}{c_k} \right)^2 \right] \tag{9}$$

where a, b, and c are the function's peak value, the corresponding horizontal coordinate position when the peak value is obtained, and the half-width information, respectively.

1) Starting travel moment

The starting travel moment is closely tied to the type of travel chain, and in order to accurately forecast the demand for EV charging and switching, it is essential to separately analyze and process the starting travel moments of different travel chains. Since travel chain 1 and travel chain 3 both pass through the work area, this paper has processed the starting travel moments of both together.

2) Parking time

The stopping time of electric vehicles is closely tied to the travel chain and the type of functional area: generally, the stopping time tends to be longer in residential areas and work areas, and shorter in other areas. Travel chain 2 has longer dwell times in other areas, while travel chain 3 has shorter dwell times in other areas. The probability distribution of the dwell time of EVs across each region in different travel chains is shown in Fig. 3, and the dwell time (in minutes) in residential areas can be expressed as:

$$t_{ph} = 1440 - \left(t_3 - t_0 \right) \tag{10}$$

where t_3 is the moment of return to the residential area and t_0 is the starting travel moment.

3) Travel distance

The value of the probability density function parameter for travel distance is also related to the type of travel chain.

4) Initial charging state

Most electric vehicle users travel a short distance, electric vehicles are fully charged, generally can meet the user's travel needs for over 3 days. As a result, electric vehicles do not require charging on a daily basis, and the battery power is not always full charge state, but randomly distributed. In this paper, we define the initial charge state of the battery as following a normal distribution $\left(0.5, 0.1^2\right)$.

(2) Taxi Travel Characteristics

The fundamental travel characteristics of a cab encompass the starting travel time and the initial charge state. The initial travel time probability distribution of the cab is provided by NCHRP 187 (National Cooperative Highway Research Program), and the cab travel characteristic quantity is shown in Fig. 4, and the initial SOC follows a normal distribution $\left(0.5, 0.1^2\right)$.

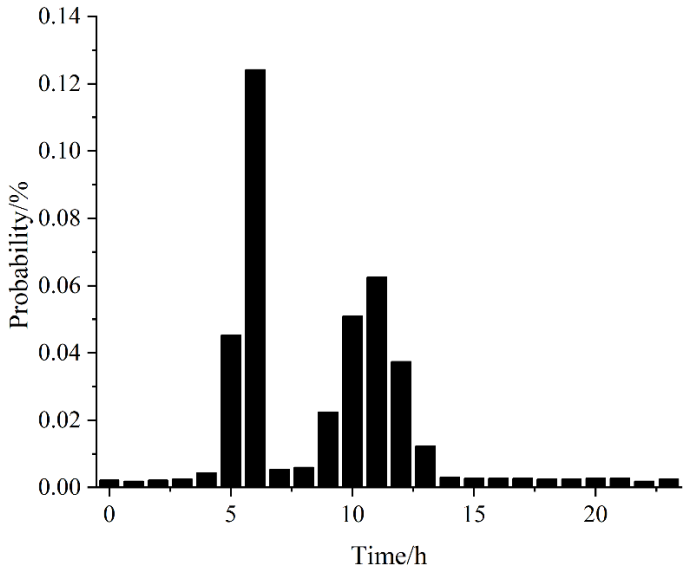

Figure 4: The probability distribution of the starting trip of a taxi

3.2 Electric Vehicle Charging and Switching Mode Decision Making

In order to avoid damage to the battery, the remaining battery capacity should not be less than a certain threshold. Considering the subjective charging anxiety of EV users, this paper sets the threshold charge C_{ap} to be uniformly distributed between 0.2C~0.3C, where C denotes the battery capacity. Upon the electric vehicle reaching the destination d, if the remaining battery level is insufficient to reach the next destination, the charging demand is generated, i.e.:

$$S_d C - \omega l_{d+1} < C_{ap} \tag{11}$$

where S_d represents the state of charge of the electric vehicle when it arrives at d place. ω denotes the power consumption per kilometer. l_{d+1} represents the distance of the next traveling segment.

If the electric vehicle meets the above charging conditions, there are three ways of supplying

electricity in this paper: slow charging, fast charging and power exchange.

(1) Slow charging method

If the electric vehicle arrives at destination d with insufficient remaining power to complete the next trip, and in the stopping time, selecting the slow charging method can fulfill the requirements of the next trip, i.e.:

$$S_d + P_1 t_{cd} \geq C_{ap} + \omega l_{d+1} \tag{12}$$

where P_1 is the charging power associated with the slow charging mode. t_{cd} denotes the charging duration at destination d.

(2) Fast charging mode

The criterion for selecting fast charging is as follows: during the stopping time, the amount charged through the slow charging mode falls short of completing the next trip, while the fast charging mode can meet the demand, i.e.:

$$S_d C + P_2 t_{cd} \geq C_{ap} + \omega l_{d+1} \tag{13}$$

where P_2 is the charging power associated with the fast charging mode. Upon selecting the charging mode, the charging duration t_{cd} at d place is divided into two cases.

1) If the battery can not be full during the stopping time, then the charging duration is equal to the stopping duration t_{pd}, i.e.:

$$t_{cd} = t_{pd} \tag{14}$$

2) If the battery reaches full charge within the stopping time, the corresponding charging duration is:

$$t_{cd} = \frac{\left(1 - S_d C\right)}{P_c} \tag{15}$$

where P_c is the charging power.

(3) Power exchange mode

The conditions for the user to choose the power exchange are: during the stopping time, even if the fast charging mode is chosen, the charged amount is not enough to complete the next trip, at this time, no charging is done at the d place, and the user chooses to exchange the power at the nearest power exchange station on the way to the next trip.

Private cars can choose one of the three types of energy supply methods to replenish electricity according to the charging and switching decision-making mechanism, while cabs, considering profitability and other factors, choose the switching method that takes the shortest time to replenish electricity. In addition, due to the influence of geographic space, the quantity of charging piles constructed in certain areas is unable to satisfy the charging requirements of users due to geospatial constraints, and some users are unable to charge after arriving at their destinations, so they can only choose the power exchange method to replenish electric energy during their next trip.

3.3 Spatial and temporal prediction of grid load under EV charging and switching mode

3.3.1 Probability distribution fitting models

The probability distribution forms to be used in this paper include the lognormal distribution, the higher-order Fourier distribution function, the mixed-sum normal distribution function, and the first-order or multiorder Gaussian distribution function, of which the latter three expressions are, respectively:

$$\begin{aligned} f(x) &= a_0 + a_1 \times \cos(xw) + b_1 \times \sin(xw) \\ &\quad + \cdots + a_n \times \cos(nxw) + b_n \times \sin(nxw) \end{aligned} \tag{16}$$

$$f(x) = \sum_{i=1}^{n} p_i \frac{1}{\sqrt{2\pi}\sigma_i} \exp\left(-\frac{(x-\mu_i)^2}{2\sigma_i^2} \right) \tag{17}$$

$$\begin{aligned} f(x) &= a_1 \exp\left[-\left(\frac{x-b_1}{c_1} \right)^2 \right] + a_2 \exp\left[-\left(\frac{x-b_2}{c_2} \right)^2 \right] + \\ &\quad \cdots + a_n \exp\left[-\left(\frac{x-b_n}{c_n} \right)^2 \right] \end{aligned} \tag{18}$$

In Eqs. (16)~(18), x denotes the return moment. μ_i, σ_i, p_i are the i th normal distribution mean, standard deviation, and coefficient $\sum p_i = 1$, respectively. $a_0 \cdots a_n$, $b_0 \cdots b_n$ denote the coefficients.

To reflect the fitting effect, the coefficient of determination R^2 and the correction coefficient of determination R_a^2 are used to quantify the fitting effect together, and the closer the two parameters are to 1, the better the fitting effect is indicated. The correction coefficient R_a^2 is obtained after normalizing R^2, and the two are defined as:

$$R^2 = \frac{E_{ssr}}{E_{sst}} = \frac{\sum_{i=1}^{n} (\hat{y}_i - \bar{y}_i)^2}{\sum_{i=1}^{n} (y_i - \bar{y}_i)^2} \tag{19}$$

$$R_a^2 = 1 - (1 - R^2) \times \frac{n-1}{n-p-1} \tag{20}$$

In Eqs. (19) to (20), $\hat{y}_i$ is the output of the fitted curve. $\bar{y}_i$ is the original data mean. y_i is the original data. n is the number of data. p is the number of fitting parameters.

The charging onset moment and charging onset SOC of a private car on a rest day are taken as examples to compare the fitting results under different distribution forms. The comparison finds that the charging onset moment is better fitted with a third-order Fourier distribution function, while the charging onset SOC better obeys a normal distribution.

3.3.2 Monte Carlo Charging Load Prediction Models

In this section, a charging load prediction model is developed utilizing the Monte Carlo simulation approach of momentary charging probability. To begin with, a mathematical probability model of factors influencing charging load prediction is constructed. Subsequently, the charging probability distribution function of each moment is derived and the charging probability of the corresponding moment is computed. Finally, the charging load is obtained by multiplying the charging probability with the charging power. The simulation flow is shown in Fig. 5.

Let $\gamma_{t0}=1$ denote the on-grid state at the moment of t_0 and $\gamma_{t0}=0$ denote the off-grid state. Dividing a 24h day into 96 time slots in steps of 15min, the charging probability of a vehicle in t_0 time slot is:

$$p\left(\gamma_{t0}=0\right)=F_s\left(t_s>t_0, t_s+T_{char}\le t_0+96\right)+F_s\left(t_s+T_{char}\le t_0\right) \tag{21}$$

$$p\left(\gamma_{t0}=1\right)=1-F_s\left(t_s>t_0, t_s+T_{char}\le t_0+96\right)-F_s\left(t_s+T_{char}\le t_0\right) \tag{22}$$

In Eqs. (21)~(22), t_s is the starting charging moment of the vehicle. F_s represents the probability distribution function corresponding to the starting charging moment t_s. T_{char} is the EV charging duration.

is the charging load:

$$P_{t0}=P_c\left(t_0\right)\times p\left(\gamma_{t0}=0\right)+P_c\left(t_0\right)\times p\left(\gamma_{t0}=1\right)=P_c\left(t_0\right)\times p\left(\gamma_{t0}=1\right) \tag{23}$$

where P_{t0} denotes the charging load at the moment t_0. $P_c(t_0)$ is the charging power at the moment t_0, when $\gamma_{t0}=0$, $P_c(t_0)=0$.

The total cluster EV load:

$$P^{total}=\sum_{i=1}^{N}\sum_{j=1}^{24} f_{ij}P_{cij} \tag{24}$$

where P^{total} denotes the overall charging load. N is the number of EVs. P_{cij} denotes the charging load of the i th vehicle in the j th hour.

The variance coefficient is used to determine whether the simulation results converge or not, i.e.:

$$\beta_j=\frac{\sqrt{V_j(\bar{L})}}{\bar{L}_j}=\frac{\sigma_j(\bar{L})}{\sqrt{k}\bar{L}_j} \tag{25}$$

where β_j, $V_j(\bar{L})$, $\bar{L}_j$, $\sigma_j(\bar{L})$ are the coefficient of variance, variance, expectation, and standard deviation of the prediction outcomes, respectively. k denotes the number of iterations. It will be $\max\left\{\beta_j\right\}<0.05\%$ judged that the simulation results converge and the simulation can be ended.

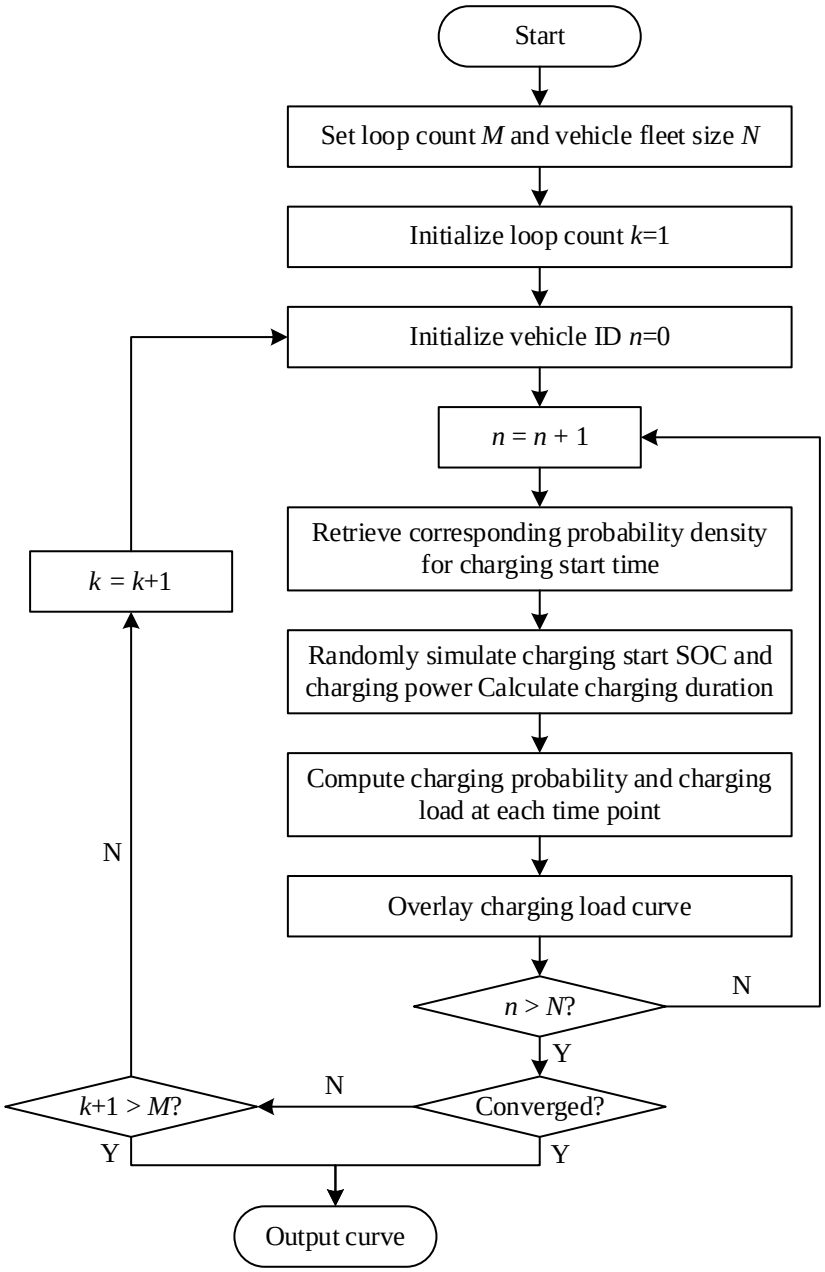

Figure 5: Monte carlo simulation process

4 Example analysis

4.1 Parameterization of the algorithm

Taking a certain region as the simulation object, the proportion of private cars to cabs in the region is approximately 10:1, and the fleet size of private cars is configured at 11,000 and the fleet size of cabs is configured at 1,100 in this paper's calculation example. The battery rated capacity of the electric vehicle is 22kWh, the initial charging state soc_0 satisfies the normal distribution $N(0.46, 0.17)$, and the upper and lower thresholds of the battery charging state soc_{max} and soc_{min} are 0.92 and 0.11, respectively. The fast charging pile operates at 52kW, and the slow charging pile operates at 3.2kW, and the charging efficiency is 0.96.

The actual parameters of the electric vehicle are selected based on data from four representative days in spring, summer, autumn and winter, respectively, in which the reference temperature in spring and autumn is 22℃, the summer reference temperature is 36℃, and the winter reference temperature is 0℃, and the energy consumption per unit distance of the electric vehicle in spring and autumn is 18kW/100km, and the energy consumption of the air conditioning system is estimated at 22kW/100km in summer and winter. The minimum acceptable remaining battery level for the electric vehicle user is configured at 0.5 times soc_0. The threshold soc_{th} is set to 0.5 times soc_0, and the upper bound of mileage anxiety tolerance follows the uniform distribution $U(soc_0, 0.9)$. The operation end time of cab users satisfies the uniform distribution U(20:00, 24:00).

4.2 Electric Vehicle Charging and Switching Demand Calculation

4.2.1 Electricity consumption per unit mile for vehicles

The correlation between energy consumption per unit distance of electric vehicles and temperature and driving speed is shown in Fig. 6, which shows that the energy consumption per kilometer of electric vehicles reaches its minimum at 25℃, and the energy consumption per kilometer will progressively rise with either an increase or decrease in temperature. And as the speed increases, the power consumption of the electric vehicle will gradually decrease.

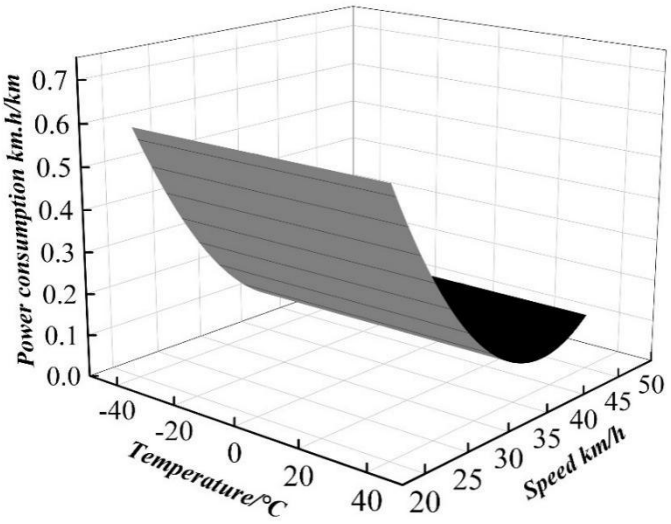

Figure 6: Electricity consumption per kilometre

4.2.2 Vehicle Charging Requirements in Parked Conditions

Adopt the mode of stop-and-go charging for the user's parking state charging demand, and make the following assumptions.

(1) Set the user's parking time as the charging time.

(2) The user's charging duration is set as the duration of the parking state or the time required for the battery to transition from the current charge level to a fully charged state.

(3) The electric vehicle's travel speed is configured at 50km/h and the outdoor temperature is 30℃.

(4) The power level must reach 42% of the total power level at the moment the user leaves.

(5) Due to the large difference in parking time between recreational areas, work areas and residential areas, the corresponding charging mode is selected according to the length of stay. The rapid charging power is configured at 30 kW, and the conventional charging power is

configured at 3 kW. The charging demand of each parking state is shown in Fig. 7, comparing the charging demand of different parking states, the charging demand within the residential area is concentrated in the period of 14:30-16:30, the charging demand within the work area is concentrated in the period of 10:00-15:00, and the charging demand within the recreational area is concentrated in the period of 11:00~14:00. Charging demand increases from around 6:00 p.m. After 20:00 p.m., there is less charging demand in both the work area and residential area, and there is still charging demand in the recreational area, but it maintains a decreasing trend.

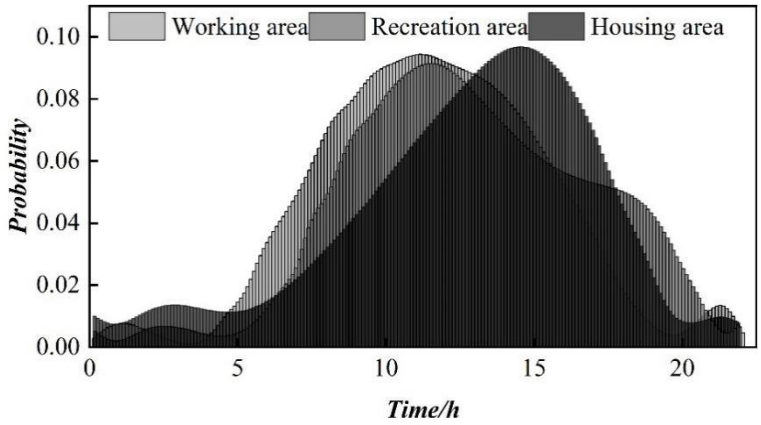

Figure 7: Demand charging state of each parking area

4.2.3 Demand for power exchange while the vehicle is in motion

Based on the above assumptions, it is concluded that the power consumption of EVs is 0.211kW·h per kilometer, and the maximum driving distance on full charge is 166km.There are 3578 EVs in the simulated EVs in the paper that have the demand for power change. Comparing the demand for power change in the three scenarios is shown in Fig. 8, in which most of the demand for power change after leaving the recreation area is concentrated in driving between 70km and 88 km, and most of the demand for power change after leaving the work area is concentrated in driving between 56km and 68km, and continues to decrease. After leaving the residential area, most of the demand for changing points is concentrated around 111 km of driving, increases continuously from around 80 km, and decreases from around 105 km. Comparing the demand for point-of-exchange in the three cases, it can be seen that the exit curves exhibit considerably varied distributions, with different peaks, and the charging duration of the stay in each area has a greater impact on the demand for point-of-exchange.

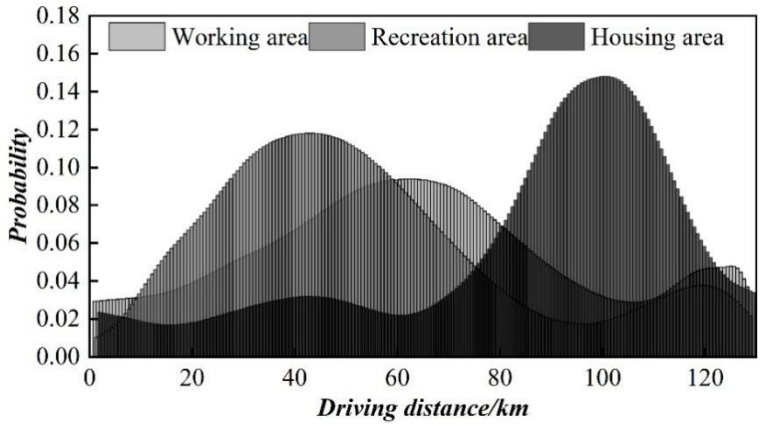

Figure 8: Battery swapping demand in driving state

4.3 Electric Vehicle Charging and Switching Demand Forecast Results and Analysis

4.3.1 Demand forecast for charging

The daily charging load of electric vehicles across different seasons is illustrated in Figure 9. The results indicate that the peak charging load is centrally distributed at 14:00~23:00, and the charging load fluctuates more on weekdays with higher total load compared with the charging load on double holidays. Due to the effect of temperature variations on electric vehicle energy consumption and battery capacity in different seasons, the charging load has obvious seasonal characteristics, and the charging load is greater in winter and summer, and the peak charging load appears earlier.

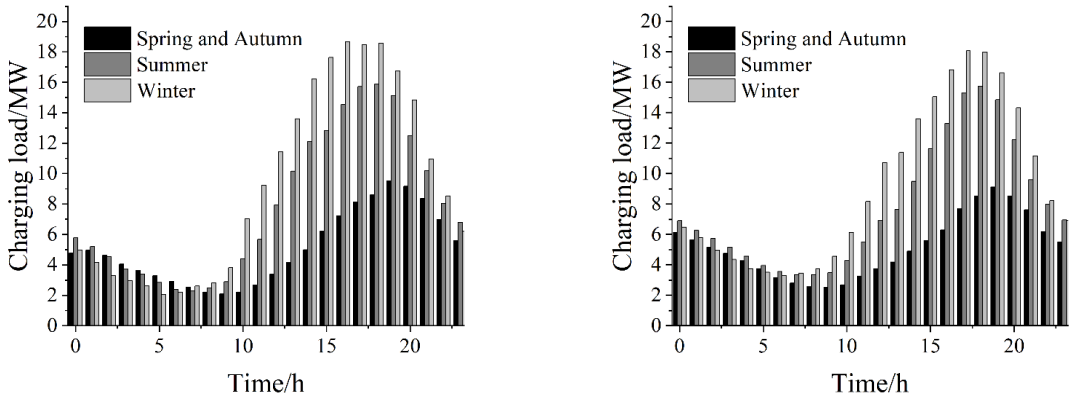

(a) Work day (b) Two-day weekend

Figure 9: Electric car daily charging load in different seasons

As an example, the charging loads of both private cars and cabs are further analyzed on weekdays, and the respective charging loads of private cars and cabs on weekdays are shown in Fig. 10, with Figs. (a) and (b) showing private cars and cabs respectively. The quantity of private cars introduced in this section is 10 times that of cabs, while the difference between the peak charging loads of the two is small, which is mainly due to the fact that cabs have a longer trip chain and a larger electricity demand, so the total load difference is smaller. At the same time, the seasonal difference due to temperature is more significant due to the high electricity demand of cabs.

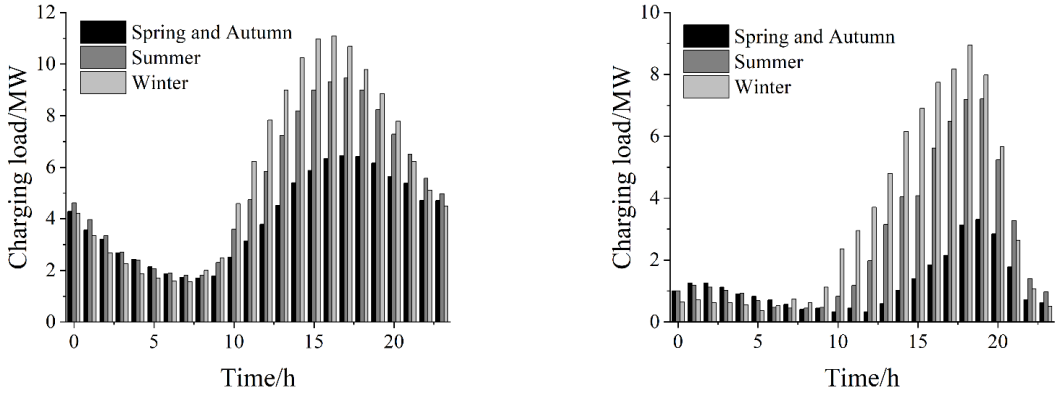

(a) Private car (b) Taxi

Figure 10: Private car and taxi charging load

Taking spring and fall as an example, we further analyze the changes of daily EV charging load in different areas, the peak charging load within residential areas is concentrated during 18:00~02:00 the next day, and the peak charging load time on weekdays is about 1 hour earlier than that on weekends and public holidays. The charging load in commercial and recreational areas fluctuates considerably between weekdays and weekends, with larger peaks in commercial and recreational areas on weekdays and obvious peaks and valleys, and smaller fluctuations in charging loads on weekdays and weekends, with a long time span. The charging load in the enterprise office area is mainly distributed in the daytime working hours, and the charging load on weekdays is considerably lower than that on working days. The distribution of charging load in the public service area is similar to that of the enterprise office area.

4.3.2 Demand forecast for power exchange

Different from the charging load prediction which yields the charging power, the power exchange demand prediction gets the number of batteries replaced at the moment of power exchange occurrence, and Figure 11 shows the daily power exchange demand in different regions in different seasons. It can be seen that the power exchange demand pattern resembles the charging load curve, and the power exchange demand is centrally distributed in the period from 14:00 to 23:00. Compared with double holidays, the power exchange demand fluctuates more on weekdays, and the total demand is higher. Demand for power exchange also has obvious seasonal characteristics, with greater demand for power exchange in winter and summer, and the peak time appearing earlier.

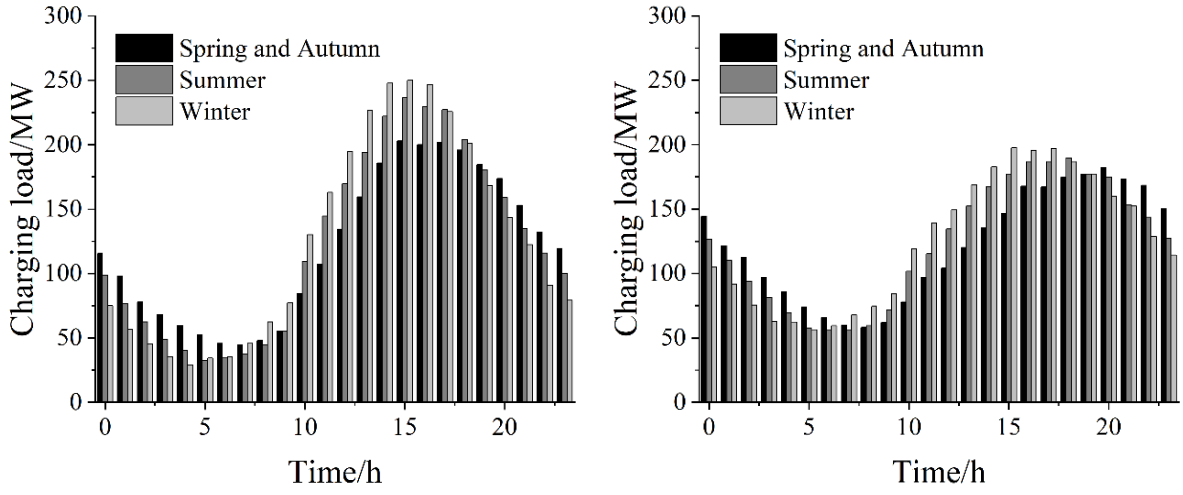

(a) Work day (b) Two-day weekend

Figure 11: Change of electricity demand in different regional days of different seasons

5 Conclusion

A Monte Carlo prediction model grounded in momentary charging probability is employed to simulate the spatio-temporal distribution of electric vehicle charging load. The charging and switching demands of four main EV states, including residential area parking state, work area parking state, recreational area parking state, and driving state, are simulated and analyzed. The results show that:

(1) Differences in the starting and stopping states, driving mileage, and length of stay of electric vehicles will result in varying charging and switching needs of the vehicles.

(2) Different states will lead to different charging and switching demands, and the same charging demand of the same state has large differences in different time periods.

(3) User driving habits and the duration of stay in each state exert a considerable influence on the demand for power exchange in the driving state, so the demand for power exchange generated by the driving state of electric vehicles must be accounted for in practical planning.

(4) Compared with double holidays, the power exchange demand on weekdays fluctuates more and the overall demand is greater. The charging and switching demand also has obvious seasonal characteristics, with greater demand for switching in winter and summer, and the peak time appearing earlier.

The proposed method relies on the establishment of the vehicle spatio-temporal state chain model, and adopts the idea of state-to-state transition to simulate the vehicle travel process, which is convenient for the subsequent analysis of the EV charging and switching station siting and capacity determination. However, the fixed speed is used in the calculation of vehicle traveling power consumption, which has some limitations, so the subsequent research can further improve the vehicle traveling speed.

Funding

This research was supported by the Study on power load characteristics in Sichuan under industrial upgrading and extreme weather influence (52199623000H).

About the Authors

Tao Luo, male, Han, born in Chongqing, January 1968, master's degree, senior engineer, research direction: energy economy, power demand analysis and forecasting, etc.

Bo Li, male, Han, born in Leshan, Sichuan, May 1986, master's degree, senior engineer, research direction: energy economy, power demand analysis and forecasting, etc.

Ruiguang Ma, male, Han, born in Jining, Shandong, May 1987, Ph.D., senior engineer, research direction: energy policy, energy economy, power market, etc.

Tiannan Ma, male, Han, born in Wuzhong, Ningxia, July 1992, Ph.D., senior engineer, research direction: energy policy, energy economy, power market, etc.

Qiang Ye, male, Han, born in Bazhong, Sichuan, August 1982, master's degree, senior engineer, research direction: power planning, energy economy, power market, etc.

Hao Luo, female, Han, born in Neijiang, Sichuan, January 1997, master's degree, engineer, research direction: energy policy, energy economy, power market, etc.

References

[1] Abo-Khalil, A. G., Abdelkareem, M. A., Sayed, E. T., Maghrabie, H. M., Radwan, A., Rezk, H., & Olabi, A. G. (2022). Electric vehicle impact on energy industry, policy, technical barriers, and power systems. International Journal of Thermofluids, 13, 100134.

[2] Yao, S., Bian, Z., Hasan, M. K., Ding, R., Li, S., Wang, Y., & Song, S. (2023). A bibliometric review on electric vehicle (EV) energy efficiency and emission effect research. Environmental Science and Pollution Research, 30(42), 95172-95196.

[3] Suraharta, I. M., Djajasinga, N. D., Wicaksono, M. B. A., Akbar, R. A., Priono, N. J., Yusuf, M. A., & Gugat, R. M. D. (2022). Electric vehicle policy: the main pillar of

Indonesia's future energy security. International Journal of Science and Society, 4(4), 142-156.

[4] Kurniawan, D. (2024). Investigating the effectivity of promoting electric vehicle to reduce air pollution: An analysis of Indonesia power plants. Journal of Law and Sustainable Development, 12(2), e2731-e2731.

[5] Lu, M., & Sun, J. (2024). Collaborative optimization algorithm for electric vehicle industry chain based on regional economic development needs. International Journal of Emerging Electric Power Systems, 25(5), 593-602.

[6] Zhang, Z., Shi, H., Zhu, R., Zhao, H., & Zhu, Y. (2021). Research on electric vehicle charging load prediction and charging mode optimization. Archives of Electrical Engineering, 399-414.

[7] Zabihia, A., & Parhamfarb, M. (2024). Empowering the grid: toward the integration of electric vehicles and renewable energy in power systems. International Journal of Energy Security and Sustainable Energy, 2(1), 1-14.

[8] Hadian, E., Akbari, H., Farzinfar, M., & Saeed, S. (2020). Optimal allocation of electric vehicle charging stations with adopted smart charging/discharging schedule. IEEE Access, 8, 196908-196919.

[9] Feng, J., Yang, J., Li, Y., Wang, H., Ji, H., Yang, W., & Wang, K. (2021). Load forecasting of electric vehicle charging station based on grey theory and neural network. Energy Reports, 7, 487-492.

[10] Tikka, V., Haapaniemi, J., Räisänen, O., & Honkapuro, S. (2022). Convolutional neural networks in estimating the spatial distribution of electric vehicles to support electricity grid planning. Applied Energy, 328, 120124.

[11] Zhang, Q., Lu, J., Kuang, W., Wu, L., & Wang, Z. (2024). Short-term charging load prediction of electric vehicles with dynamic traffic information based on a support vector machine. World Electric Vehicle Journal, 15(5), 189.

[12] Nogueira, T., Magano, J., Sousa, E., & Alves, G. R. (2021). The impacts of battery electric vehicles on the power grid: A Monte Carlo method approach. Energies, 14(23), 8102.

[13] Yi, T., Zhang, C., Lin, T., & Liu, J. (2020). Research on the spatial-temporal distribution of electric vehicle charging load demand: A case study in China. Journal of Cleaner Production, 242, 118457.

[14] Mao, M., Wu, J., Yang, C., Wang, Y., Du, Y., Zhu, M., ... & Zhang, L. (2024, June). Spatial-Temporal Prediction of Schedulable Capacity of Electric Vehicles Based on Graph Convolutional Network With Spatial-Attention. In 2024 IEEE 15th International Symposium on Power Electronics for Distributed Generation Systems (PEDG) (pp. 1-6). IEEE.

[15] Inci, M., Çelik, Ö., Lashab, A., Bayındır, K. Ç., Vasquez, J. C., & Guerrero, J. M. (2024). Power system integration of electric vehicles: A review on impacts and contributions to the smart grid. Applied Sciences, 14(6), 2246.

[16] Pham, T. N., Oo, A. M. T., & Trinh, H. (2021). Event-triggered mechanism for multiple frequency services of electric vehicles in smart grids. IEEE Transactions on Power Systems, 37(2), 967-981.

[17] Zhang, Y., Liu, C., Rao, X., Zhang, X., & Zhou, Y. (2024). Spatial-temporal load forecasting of electric vehicle charging stations based on graph neural network. Journal of Intelligent & Fuzzy Systems, 46(1), 821-836.

[18] Zheng, W., & Lee, D. H. (2025). The spatio-temporal relationship between electric vehicle charging demand and land use: Insights from Chinese metropolitan areas. Journal of Transport Geography, 129, 104421.

[19] Chen, L., Yang, F., Xing, Q., Wu, S., Wang, R., & Chen, J. (2020, October). Spatial-temporal distribution prediction of charging load for electric vehicles based on dynamic traffic information. In 2020 IEEE 4th Conference on Energy Internet and Energy System Integration (EI2) (pp. 1269-1274). IEEE.

[20] Ge, X., Shi, L., Fu, Y., Muyeen, S. M., Zhang, Z., & He, H. (2020). Data-driven spatial-temporal prediction of electric vehicle load profile considering charging behavior. Electric Power Systems Research, 187, 106469.